Ab initio multicenter tight-binding model for molecular-dynamics simulations and other applications in covalent systems

Otto F. Sankey and David J. Niklewski
Department of Physics, Arizona State University, Tempe, Arizona 85287-1504
(Received 21 February 1989)

A new, approximate method has been developed for computing total energies and forces for a variety of applications including molecular-dynamics simulations of covalent materials. The method is tight-binding-like and is founded on density-functional theory within the pseudopotential scheme. Slightly excited pseudo-atomic-orbitals are used to derive the tight-binding Hamiltonian matrix in real space. The method is used to find the electronic states and total energies for a variety of crystalline phases of Si and the Si_2 molecule. Excellent agreement is found with experiment and other first-principles methods. As simple applications of the method, we perform a molecular-dynamics simulated-annealing study of the Si_3 molecule to determine the ground-state configuration, and a molecular-dynamics simulation of the spectral density function of the Si_2 molecule at high and low excitation levels.

I. INTRODUCTION

Molecular dynamics is a technique which can be useful for simulating vibrations of molecules and solids, the growth of a crystal or interface, the interaction between an adatom and surface, defect reactions in crystals, migration of atoms in solids, and a wide range of other time-dependent phenomena. In this technique, the many-body classical equations of motion are solved as a function of time, and the physical process can be studied in real time. The equations of motion are prescribed once the instantaneous forces are given.

The forces between atoms in covalent solids is more intricate than a sum of two-body forces because the strength of the covalent bond is quantum-mechanically derived and depends on the local environment. Potentials have been devised[1] which mimic these nonlocal many-atom effects. However, the many-body effects are clearly rooted in the quantum electronic structure of the material and a superior method is to obtain these forces directly from the electronic structure.

The purpose of this paper is to develop a first-principles electronic-structure method which approximates very closely a rigorous calculation of these forces, yet is simple enough to be used for a wide variety of purposes, including molecular-dynamics simulations of covalent materials. We have tested the static energetics thoroughly in Si, and have performed molecular-dynamics and molecular-dynamics simulated-annealing studies of small Si clusters. The method is framed within a first-principles tight-binding approximation, making it versatile and easy to use, and is executed entirely in real space, and so periodicity is not necessary. It can be adapted for use in supercells, slabs, clusters, or within a Green's-function technique.

Our approach is to use a number of physically motivated approximations within the framework of a well-established first-principles theory, to retain accuracy and transferability, yet still achieve the goal of simplifying the computation of the total energy and atomic forces. The theoretical foundation that we use is density-functional theory within the local-density and pseudopotential approximations.

The outline of the paper is as follows. In Sec. II we give a brief review of the tight-binding approximation as it is currently used and point out its advantages and its shortcomings. Section III develops our theory and the three major approximations that are made which simplify the theory without sacrificing reliability. The details of how the one-electron Hamiltonian tight-binding matrix elements are determined are given in Sec. IV. In Sec. V, we discuss the application of the Hellmann-Feynman theorem to evaluate the atomic forces. Applications and tests of the method are given in Sec. VI, and include the properties of bulk Si, the phase diagram of Si in five different phases, and molecular-dynamics simulations of small Si clusters. Finally in Sec. VII we give our conclusions.

II. REVIEW OF TIGHT-BINDING MODELS

We begin by a brief review of tight-binding models as they are typically used in current applications. Since most tight-binding models are only loosely defined in terms of a fundamental electronic-structure theory, there is no unique tight-binding theory. Our discussion will try only to give the essence of the method, and not follow any single model. The tight-binding models which fit into the class of models we discuss are those used, for example, by Harrison[2] and others.[3–11]

The tight-binding model is an approximate method to determine the electronic structure of the system. An atomiclike orbital basis $|\phi_\mu\rangle$ is imagined in which matrix elements of a one-electron Hamiltonian, $h_{\mu\nu}$, are assumed to be known. The electronic energy eigenstates ψ_i are expanded as a linear combination of the atomiclike states as

$$|\psi_i\rangle = \sum_\mu a_\mu^i |\phi_\mu\rangle \ . \tag{1}$$

The expansion coefficients are determined from the one-electron eigenvalue equation

$$\sum_\nu h_{\mu\nu} a_\nu^i = \varepsilon^i a_\mu^i \ , \tag{2}$$

where ε^i is the electronic eigenvalue for state i.

A major advantage of the tight-binding method is that the chemistry is taken into account in a physical and quantum-mechanical way. The electronic states may be relatively localized or spread throughout the system, and bonds are formed with many-atom noncentral effects naturally included. The bonds formed have a variety of strengths and symmetries, such as π or σ type.

The tight-binding model *per se* gives no definite form for the total energy of the system. The eigenvalues ε^i are one-electron eigenvalues, and by themselves do not give the total electronic energy. They do represent an important contribution to the total energy, so that the total energy is usually taken to have the form

$$E_{\rm tot} = 2 \sum_{i\ \rm occ} \varepsilon^i + \tfrac{1}{2} \sum_{l,l'}{}' V_R(|\mathbf{R}_l - \mathbf{R}_{l'}|) \ . \tag{3}$$

The first term is the "band-structure" energy obtained by summing the one-electron eigenvalues over occupied states, which are assumed doubly occupied here. The second term is a repulsive two-body (central) potential between the atoms located at $\mathbf{R}_l$ and $\mathbf{R}_{l'}$. The band-structure term draws the atoms together and the repulsive term separates them so that an equilibrium is reached.

A number of empirical forms for $V_R(\mathbf{R}_l - \mathbf{R}_{l'})$ have been chosen. Popular choices are an inverse power law,[12] $A/|\mathbf{R}_l - \mathbf{R}_{l'}|^4$, or a polynomial form about equilibrium.[3] The parameters of the short-ranged repulsive potential V_R, as well as the tight-binding Hamiltonian matrix elements themselves, $h_{\alpha\beta}$, are empirically fitted to experiment or first-principles theories. This seriously limits the reliability of the method and confines it to physical situations that are not too different from those in which the parameters are fitted. For instance, small vibrational modes might be expected to be generally well modeled, but an interstitial impurity in an otherwise perfect crystal ought to be treated cautiously. The interstitial impurity finds itself in a very different bonding environment with a different number of nearest neighbors, bond lengths, and symmetry. In general, the tight-binding parameters are not necessarily transferable from one structure to another by a simply distance scaling. The on-site matrix elements are not necessarily constant and the parameters appear to be dissimilar for carbon in the diamond and graphite phases.[13] Used cautiously, however, the tight-binding model has been extremely useful in a wide variety of applications.

The tight-binding method has obvious advantages, but it suffers the following major difficulties: (i) the tight-binding matrix elements $h_{\mu\nu}$ typically are between very near neighbors only, and must be determined empirically; (ii) the matrix elements do not contain explicitly three-center terms $\langle\phi_\mu|V(\mathbf{r}-\mathbf{R}_l)|\phi_\nu\rangle$, where V is the one-electron potential in the Hamiltonian located on atom $\mathbf{R}_i$, different from the positions of orbitals $|\phi_\mu\rangle$ and $|\phi_\nu\rangle$; (iii) the orbitals $|\phi_\mu\rangle$ and $|\phi_\nu\rangle$ are not orthogonal but are treated as such; and (iv) the form of the total energy has little fundamental basis, and must be fitted to a physical problem whose solution is known. One can argue that, since current tight-binding models are empirical, unspecified transformations can be performed which repair some of the difficulties above. For instance, the orthogonality of the orbitals can be achieved by a Löwdin[14] tansformation that transforms the overlap and the Hamiltonian matrices. Similarly, since the Hamiltonian matrix elements are fitted, one could argue that in some effective manner three-center terms are included in the Hamiltonian matrix elements. However, these approximate repairs are only true for the system which is fitted. Once the system is changed to the system of interest, a different Löwdin transformation must be used, and new or different three-center Hamiltonian matrix elements have emerged.

We now go on to discuss our tight-binding model, which, to maintain the advantages of tight-binding models, is still approximate, does not require any fitting to experimental data, and has none of the major difficulties of (i)–(iv) outlined above.

III. THEORY

A. Theoretical foundation

The theoretical foundation of our theory is density-functional theory, within the local-density approximation (LDA) and the nonlocal pseudopotential scheme. Within these approximations, the total energy of the system is written as

$$\begin{aligned} E_{\rm tot} = {} & 2 \sum_i \left\langle \psi_i \left| \frac{p^2}{2m} \right| \psi_i \right\rangle \\ & + 2 \sum_l \langle \psi_i | [V_{\rm ion}(\mathbf{r}-\mathbf{R}_l) + V_{\rm NL}(\mathbf{r}-\mathbf{R}_l)] | \psi_i \rangle \\ & + \frac{e^2}{2} \int\int \frac{n(\mathbf{r}) n(\mathbf{r})}{|\mathbf{r}-\mathbf{r}'|} d^3r\, d^3r' + \int n(\mathbf{r}) \varepsilon_{\rm XC}(n) d^3r \\ & + \frac{e^2}{2} \sum_{ll'}{}' \frac{Z_l Z_{l'}}{|\mathbf{R}_l - \mathbf{R}_{l'}|} \ , \end{aligned} \tag{4}$$

which correspond, respectively, to the kinetic energy, the electron interaction with the ionic and nonlocal pseudopotentials, the electron-electron Hartree interaction, the exchange-correlation interaction within the LDA, and the ion-ion interaction. We will assume a spin-unpolarized system with doubly occupied orbitals. The exchange-correlation (XC) functional $\varepsilon_{\rm XC}(n)$ is a functional of the electron number density n, and we use the Ceperley-Alder form,[15] as parametrized by Perdew and Zunger.[16]

Within the pseudopotential approximation only the valence electrons are included, and Z_l is the number of valence electrons of the atom located at R_l (four for Si). The pseudopotential used are of the nonlocal norm-

conserving Hamann-Schlüter-Chiang type.[17] The pseudopotential is split into a long-range core potential and a nonlocal (angular-momentum-dependent) potential,

$$V_{\rm ps}(r)=V_{\rm core}(r)+V_{\rm NL}(r)\ , \tag{5}$$

where

$$V_{\rm NL}(r)=\sum_{l=0}^{2} V_l(r)\hat{P}_l \tag{6}$$

and $\hat{P}_l$ is the projector onto angular momentum l. The core pseudopotential $V_{\rm core}$ is parametrized in the form of Bachelet *et al.*,[18] where the true nuclear and core electron charges are replaced by pseudonuclear Gaussian charges to yield

$$V_{\rm ion}(r)=\frac{-Ze^2}{r}\{C_1{\rm erf}[(\alpha_1)^{1/2}r]+C_2{\rm erf}[(\alpha_2)^{1/2}r]\}\ , \tag{7}$$

where $C_1+C_2=1$. For large r, i.e., outside the core region, this approaches the correct ionic limit. The nonlocal pseudopotential is short ranged and is fitted to

$$V_l(r)=\sum_{i=1}^{3}[A_i(l)+r^2A_{i+3}(l)]e^{-\alpha(l)r^2}\ . \tag{8}$$

The local and nonlocal pseudopotentials are shown in Fig. 1 for Si. Values for the fitting parameters C_i, $\alpha_i^{\rm core}$, $A_i(l)$, and $\alpha(l)$ are tabulated in Ref. 19.

The electron density is given by the sum over occupied one-electron states ψ_i, $n(\mathbf{r})=2\sum_{i\ {\rm occ}}|\psi_i(\mathbf{r})|^2$. The one-electron eigenstates satisfy the self-consistent Hohenberg-Kohn-Sham[20] equations,

$$\left[\frac{p^2}{2m}+\sum_l[V_{\rm ion}(\mathbf{r}-\mathbf{R}_l)+V_{\rm NL}(\mathbf{r}-\mathbf{R}_l)]+e^2\int\frac{n(\mathbf{r})}{|\mathbf{r}-\mathbf{r}'|}d^3r'+\mu_{\rm XC}(n(r))\right]\psi_i(\mathbf{r})=\varepsilon_i\psi_i(\mathbf{r})\ , \tag{9}$$

where $\mu_{\rm XC}(n)=(d/dn)n\varepsilon_{\rm XC}(n)$ is the XC potential.

The total energy [Eq. (4)] can be simplified by using the eigenvalues of Eq. (9) to yield the well-known result

$$E_{\rm tot}=2\sum_{i\ {\rm occ}}\varepsilon_i+\frac{e^2}{2}\left[\sum_{ll'}{}'\frac{Z_lZ_{l'}}{|\mathbf{R}_l-\mathbf{R}_{l'}|}-\int n(\mathbf{r})d^3r\int\frac{n(\mathbf{r}')}{|\mathbf{r}-\mathbf{r}'|}d^3r'\right]+\int n(\mathbf{r})[\varepsilon_{\rm XC}(n)-\mu_{\rm XC}(n)]d^3r\ . \tag{10}$$

The second term is the difference between the repulsive interactions of the pseudocores and of the valence-electron densities. The electron-electron repulsion corrects for the double counting in the sum of eigenvalues. The third term is an XC correction of the electronic eigenvalues.

The resultant self-consistent theory embodied by Eqs. (9) and (10) has been used innumerably in a wide variety of applications with great success. The calculations are difficult, however, and, in particular, are limited to relatively small systems. To reduce the computational demands, Car and Parrinello[21,22] have introduced a fictitious Lagrangian technique which treats both electronic and nuclear degrees of freedom simultaneously. Their approach, in essence, makes no approximations to Eqs. (9) and (10), since the charge density is expanded in plane waves (a complete set). Their method, however, still has extremely high computing demands, but has been used on a number of systems.[23–27] Pederson *et al.*[28] have successfully introduced an all-electron density-functional method that uses floating Gaussian orbitals to reduce the size of the secular determinant derived from Eq. (9). In this respect, their method is similar to ours.

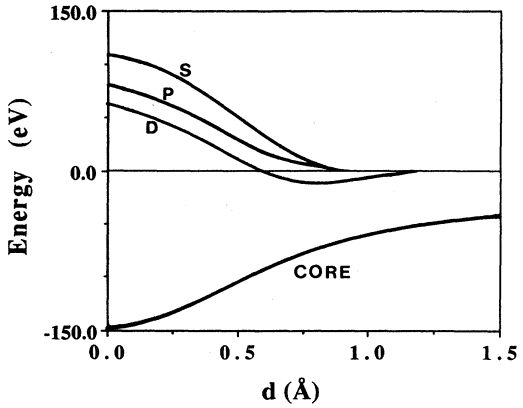

FIG. 1. The local and angular-momentum nonlocal pseudopotentials used for Si from Ref. 19. The local pseudopotential goes as $-4e^2/r$ asymptotically.

Our method reduces the secular determinant and uses Eqs. (9) and (10) in an approximate form. The major approximations are as follows: (i) substitute for the total-energy functional [Eq. (4)] a functional that has changes of the electron density from that of a sum of neutral-atom densities only to first order, (ii) approximate the self-consistent solution of Eq. (9) by a linear combination of slightly excited pseudo-atomic-orbitals, and (iii) evaluate approximately the single-particle Hamiltonian matrix elements necessary to solve Eq. (9). We now describe the first two approximations and in Sec. IV describe the evaluation of the matrix elements.

B. The approximate energy functional

The self-consistent electron density is written as

$$n(\mathbf{r})=n_0(\mathbf{r})+\delta n(\mathbf{r})\ , \tag{11}$$

where $n_0(\mathbf{r})$ is some reference density and $\delta n(\mathbf{r})$ is the difference between the reference density and the true density. In this work we take n_0 to be simply the sum of neutral-atom spherical atomic densities,

$$n_0(\mathbf{r})=\sum_l n_{\rm atom}(\mathbf{r}-\mathbf{R}_l)\ .$$

This form of the electron density is then used in the scheme introduced by Harris[29] and Foulkes,[30] where it is

assumed that $\delta n(\mathbf{r})$ is in some sense small. The neutral-atom density $n_0(\mathbf{r})$ is used in the Kohn-Sham eigenvalue equation [Eq. (9)] to generate wave functions and hence an approximate $\delta n(\mathbf{r})$ for the composite system,

$$h^0\tilde{\psi}_i=\tilde{\varepsilon}_i\psi_i \tag{12a}$$

with

$$h^0=\frac{p^2}{2m}+\sum_l[V_{\rm ion}(\mathbf{r}-\mathbf{R}_l)+V_{\rm NL}(\mathbf{r}-\mathbf{R}_l)] +e^2\int\frac{n_0(\mathbf{r}')}{|\mathbf{r}-\mathbf{r}'|}d^3r'+\mu_{\rm XC}(n_0)\ . \tag{12b}$$

Here, $\tilde{\varepsilon}_i$ and $\tilde{\psi}_i$ are the eigenvalues and wave functions, respectively, of the approximate single-particle Hamiltonian h^0. These wave functions yield an approximate density

$$\tilde{n}(\mathbf{r})=2\sum_{i\ \rm occ}|\tilde{\psi}_i(\mathbf{r})|^2=n_0(\mathbf{r})+\delta\tilde{n}(\mathbf{r})\ . \tag{13}$$

The density change $\delta\tilde{n}(\mathbf{r})$ reflects the formation of bonds and is the first-order approximation to the self-consistent bond formation given by $\delta n(\mathbf{r})$.

The energy functional is expressed to first order in $\delta\tilde{n}$. The result is similar to the exact LDA expression [Eq. (10)] and is

$$E_{\rm tot}=\varepsilon_{\rm BS}+U_{\rm SR}+\delta U_{\rm XC}\ , \tag{14a}$$

where the "band-structure" energy is

$$\varepsilon_{\rm BS}=2\sum_{i\ \rm occ}\tilde{\varepsilon}_i\ , \tag{14b}$$

the "short-ranged" potential is

$$U_{\rm SR}=\frac{e^2}{2}\left[\sum_{l,l'}{}'\frac{Z_lZ_{l'}}{|\mathbf{R}_l-\mathbf{R}_{l'}|} -\int n_0(\mathbf{r})d^3r\int\frac{n_0(\mathbf{r}')}{|\mathbf{r}-\mathbf{r}'|}d^3r'\right]\ , \tag{14c}$$

and the XC correction is

$$\delta U_{\rm XC}=\int n_0(\mathbf{r})[\varepsilon_{\rm XC}(n_0)-\mu_{\rm XC}(n_0)]d^3r\ . \tag{14d}$$

Equations (14a)–(14d) have the correct form of the electron-electron interaction to first order in $\delta\tilde{n}$. This can be seen by adding the electron-electron interaction in the band-structure term,

$$2\int\sum_{i\ \rm occ}|\tilde{\psi}_i(\mathbf{r})|^2d^3r\int e^2\frac{n_0(\mathbf{r}')}{|\mathbf{r}-\mathbf{r}'|}d^3r' =e^2\int[n_0(\mathbf{r})+\delta\tilde{n}(\mathbf{r})]\int\frac{n_0(\mathbf{r}')}{|\mathbf{r}-\mathbf{r}'|}d^3r\,d^3r'\ ,$$

to the electron-electron interaction in the short-ranged potential,

$$-\frac{e^2}{2}\int n_0(\mathbf{r})d^3r\int\frac{n_0(\mathbf{r}')}{|\mathbf{r}-\mathbf{r}'|}d^3r'\ .$$

The sum is

$$\frac{e^2}{2}\int[n_0(\mathbf{r})+2\delta\tilde{n}(\mathbf{r})]d^3r\int\frac{n_0(\mathbf{r}')}{|\mathbf{r}-\mathbf{r}'|}d^3r'=\frac{e^2}{2}\int\int\frac{[n_0(\mathbf{r})+\delta\tilde{n}(\mathbf{r})][n_0(\mathbf{r}')+\delta\tilde{n}(\mathbf{r}')]}{|\mathbf{r}-\mathbf{r}'|}d^3r\,d^3r'+O((\delta\tilde{n})^2)\ ,$$

where the first term on the right-hand side is the correct electron-electron interaction for $n(\mathbf{r})+\delta\tilde{n}(\mathbf{r})$. In a similar way the correct XC energy can be shown to be included in Eqs. (14a)–(14d) if use is made of

$$\varepsilon_{\rm XC}(n_0+\delta n)\approx\varepsilon_{\rm XC}(n_0)+\frac{\partial\varepsilon_{\rm XC}(n_0)}{\partial n}\delta n =\varepsilon_{\rm XC}(n_0)+\frac{\mu_{\rm XC}(n_0)-\varepsilon_{\rm XC}(n_0)}{n_0}\delta n\ .$$

Our approach is to use the total-energy functional of Eqs. (14a)–(14d), where the electron eigenvalues from Eq. (12a) are those of h^0. There are two major advantages of these two equations over the exact Kohn-Sham local-density equations given by Eqs. (9) and (10). The first is that the approximate single-particle equation [Eq. (12a)] is a non-self-consistent equation. The eigenvalues need to be determined only once instead of ~ 10 times as in a typical self-consistent iteration cycle. The second advantage is that four-center Coulomb integrals do not appear in the single-particle Hamiltonian or total-energy expressions. Four-center integrals only appear in the Coulomb interaction involving $(\delta\tilde{n})^2$, which are second order in $\delta\tilde{n}$ and are not included.

Harris has used the method on homonuclear dimers and finds that strong covalent bonds can be well described. More recently, Polatoglou and Methfessel[31] have tested the method on metals, Si, and an ionic compound NaCl. They find that the Harris energy functional gives surprisingly good agreement with self-consistent calculations for all materials tested (six in all). In particular, ionic compounds gave good results. It might naively be expected that keeping δn only to first order in these materials is not sufficient, but this appears not to be the case.

C. Slightly excited pseudo-atomic-orbital

Our second major approximation puts the theory in the mathematical form of the tight-binding formalism. We form matrix elements of the single-electron Hamiltonian h^0 between atomiclike orbitals. The atomiclike orbitals we use are slightly excited pseudo-atomic-orbitals $\phi_\mu^{\rm PAO}(\mathbf{r})$. The pseudo-atomic-orbitals (PAO's) are the valence-electron orbitals of the neutral ground-state atom within the pseudopotential approximation and within the local-density approximation. These are determined using a Herman-Skillman-like program.[32]

The use of PAO's in covalent materials has been tested previously for ten different materials.[19] They were found

to give a simple yet reliable and accurate picture of the total energies and electronic states in these systems. Bulk moduli, equilibrium lattice constants, vibrational optic-mode frequencies, charge densities, and band structures are well reproduced within this atomic picture. This tight-binding-like picture has also shown itself to be very useful in describing defect states of substitutional and interstitial impurity systems.[33–35]

In the work of Ref. 19, the tight-binding-like matrix elements used ground-state atomic wave functions and were found to have a very long range. It was found that at least sixth neighbors needed to be included in order to obtain reasonably accurate band structures. Even eleventh neighbors are needed in some cases. Simply neglecting the distant matrix elements led to serious errors. This is in accord with similar findings by Chen and Sher.[36]

We seek an approximation to the tight-binding-like Hamiltonian matrix elements and demand that they have a shorter range. To shorten this range, we restate the atomic problem, and impose the boundary condition that the atomic orbital vanish outside and at a predetermined radius r_c,

$$\phi^{\mathrm{PAO}}(\mathbf{r})|_{r=r_c}=0 \ . \tag{15}$$

The limit of $r_c \to \infty$ gives the true pseudo-atomic-orbital. The boundary condition of Eq. (15) has the physical effect of mixing in slight amounts of excited orbitals of the atom inside r_c; this can be seen by adding a small amount of the $2S$ wave function to the hydrogen-atom $1S$ ground state.

Exciting the orbital mimics the physical effect present in solids of increased kinetic energy due to Fermi statistics. Also, the boundary condition of Eq. (15) is superficially similar to the Wigner-Seitz boundary condition[37] that the wave function have zero derivative at the Wigner-Seitz sphere. Our boundary condition, however, makes no reference to the condensed-matter state, and applies to molecules as well.

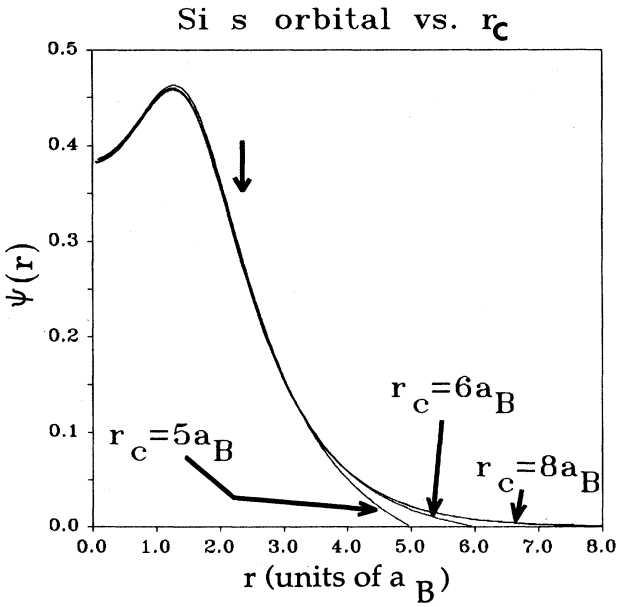

FIG. 2. The slightly excited pseudoatomic s orbital of Si for various values of r_c. The pseudo-wave-function with $r_c=8a_B$ is virtually identical to the true atomic pseudo-wave-function. The bond center is shown for crystalline Si by a vertical arrow.

The precise value of r_c chosen is not critical as long as it is well past the peak of the atomic wave function. In Fig. 2 we show the slightly excited s orbital of Si for various values of r_c. The bond-center region (defined as the half-bond-length of bulk crystalline Si) is shown. For values of r_c greater than $5a_B$, there is very little change of the atomic function in the bond region; the long wave-function tail is, however, eliminated for small values of r_c. Thus, for example, when $r_c=5a_B$, the tight-binding-like Hamiltonian matrix elements in bulk Si rigorously form a third-neighbor model. This is the value we will use for the remainder of this work.

IV. TIGHT-BINDING MATRIX ELEMENTS

We write the single-particle electronic eigenstates as a linear combination of PAO's positioned at the atomic coordinates $\mathbf{R}_l$,

$$|\psi_i\rangle=\sum_{\mu,l} a_i(\mu,l)|\phi_\mu^{\mathrm{PAO}}(\mathbf{r}-\mathbf{R}_l)\rangle \ . \tag{16}$$

We use an sp^3 basis so that $\mu=s,p_x,p_y,p_z$. The single-electron eigenvalue equation reads

$$\sum_{\nu,l'}(h^0)_{\mu\nu}^{ll'}a_i(\nu,l')=\varepsilon_i\sum_{\nu,l'}S_{\mu\nu}^{ll'}a_i(\nu,l') \ , \tag{17}$$

with eigenvalues and eigenvectors determined from the secular equation

$$\det|h^0-\varepsilon S|=0 \ .$$

The Hamiltonian matrix elements h^0 and overlap matrices are

$$(h^0)_{\mu\nu}^{ll'}\equiv\langle\phi_\mu^{\mathrm{PAO}}(\mathbf{r}-\mathbf{R}_l)|h^0|\phi_\nu^{\mathrm{PAO}}(\mathbf{r}-\mathbf{R}_{l'})\rangle \ , \tag{18a}$$

$$S_{\mu\nu}^{ll'}\equiv\langle\phi_\mu^{\mathrm{PAO}}(\mathbf{r}-\mathbf{R}_l)|\phi_\nu^{\mathrm{PAO}}(\mathbf{r}-\mathbf{R}_{l'})\rangle \ . \tag{18b}$$

The Hamiltonian h^0 is a sum of terms, which we write as

$$h^0=\frac{p^2}{2m}+\sum_l V_{\mathrm{NA}}(\mathbf{r}-\mathbf{R}_l)+\sum_l V_{NL}(\mathbf{r}-\mathbf{R}_l)+\mu_{\mathrm{XC}}(n_0) \ , \tag{19}$$

corresponding, respectively, to the kinetic energy, the Coulomb potential of a neutral atom, V_{NA},

$$V_{\mathrm{NA}}(\mathbf{r}-\mathbf{R}_l)=V_{\mathrm{ion}}(\mathbf{r}-\mathbf{R}_l)+\int\frac{n_{\mathrm{atom}}(\mathbf{r}-\mathbf{R}_l)}{|\mathbf{r}-\mathbf{r}'|}d^3r' \ , \tag{20}$$

the nonlocal pseudopotential V_{NL} of each atom, and the nonlinear XC potential. The matrix elements of h^0 are determined by adding the matrix elements of the individual terms.

In molecular dynamics or for problems with large numbers of atoms, the evaluation of the large number of integrals can place high demands on computer resources.

We now describe the method we use to circumvent these difficulties.

A. Kinetic-overlap matrix elements

The simplest matrix elements are those of the kinetic energy and the overlap. These are simply two-center integrals, and we illustrate by using the kinetic energy. We use a molecular coordinate system in which the two atoms are separated by a distance d in the z direction. The matrix element

$$T_{\mu\nu}(d)=\left\langle \phi_\mu^{\mathrm{PAO}}(\mathbf{r}) \left| \frac{p^2}{2m} \right| \phi_\nu^{\mathrm{PAO}}(\mathbf{r}-d\hat{\mathbf{z}}) \right\rangle , \tag{21}$$

then, is nonzero only between ss, $s\sigma$, σs, $\sigma\sigma$, and $\pi\pi$ orbitals. The transformation to a general coordinate system is then easily done through the Slater-Koster tables.[38] Since our orbitals are zero outside r_c, the matrix element vanishes identically for $d \geq 2r_c$. The five nonzero matrix elements of T and S are computed on a fine one-dimensional grid of distances up to $2r_c$. The value of the matrix element and its derivative at any distance are easily interpolated. The calculation of the matrix elements on the grid is done beforehand, so that calculating the matrix element for the desired geometry is a simple matter of looking it up in a table. A plot of the kinetic energy and overlap between two Si s orbitals ($r_c = 5a_B$) is shown in Fig. 3.

A technical point concerns the slightly excited PAO's. The derivative is discontinuous at r_c and the second derivative yields a δ function. This causes no unphysical properties, but mathematically gives rise to an extra surface integral, as can be seen in Green's theorem. The surface integral is avoided by performing the integral in momentum space. The kinetic-energy matrix element [Eq. (21)] becomes

$$T_{\mu\nu}(d)=\frac{1}{(2\pi)^3}\int [\phi_\mu^{\mathrm{PAO}}(\mathbf{q})]^* \frac{\hbar^2 q^2}{2m} \phi_\nu^{\mathrm{PAO}}(\mathbf{q}) e^{-i\mathbf{q}\cdot\mathbf{d}} d^3q .$$

The angular integral can be done analytically leaving only a radial integral. For example, the s-s matrix element becomes

$$T_{ss}(d)=\frac{\hbar^2}{\pi m}\int_0^\infty q^4 R_0(q) R_0(q) j_0(qd) dq , \tag{22}$$

where $R_0(q)$ is the Fourier transform of the radial wave function. The finite radius r_c gives a slight ringing to $R_0(q)$ of the form $\sin(qr_c)/(qr_c)^3$, so that the one-dimensional integral must not be cutoff in momentum space too early.

B. Neutral-atom matrix elements

The single-particle Hamiltonian h^0 contains a sum of neutral-atom potentials over all atoms, $\sum_l V_{\mathrm{NA}}(\mathbf{r}-\mathbf{R}_l)$, where

$$V_{\mathrm{NA}}(\mathbf{r}-\mathbf{R}_l)=V_{\mathrm{ion}}(\mathbf{r}-\mathbf{R}_l)+\int \frac{n_{\mathrm{atom}}(\mathbf{r}-\mathbf{R}_l)}{|\mathbf{r}-\mathbf{r}'|} d^3r' . \tag{23}$$

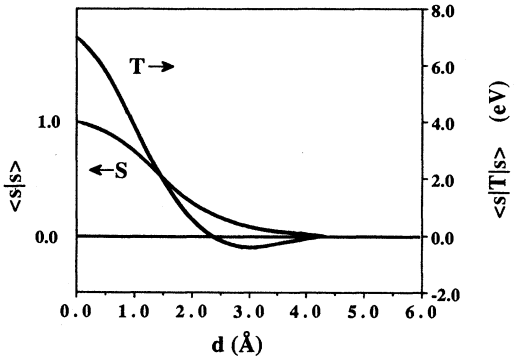

FIG. 3. The kinetic and overlap two-center tight-binding matrix elements between two Si pseudoatomic s orbitals. The orbital cutoff r_c is $5a_B$, and the matrix element is exactly zero past $10a_B$ (5.3 Å).

We will assume in all cases that outside r_c ($\gg r_{\mathrm{core}}$), V_{ion} becomes identical to $-Ze^2/r$.

The pseudonuclear charge and neutral-atom charge enclosed inside r_c cancel, so that Gauss's law requires that V_{NA} vanish outside r_c. This greatly reduces the number of nonzero matrix elements. For a general three-center neutral-atom matrix element, $\langle \phi^{\mathrm{PAO}}(\mathbf{r}-\mathbf{r}_1)|V_{\mathrm{NA}}(\mathbf{r}-\mathbf{r}_3)|\phi^{\mathrm{PAO}}(\mathbf{r}-\mathbf{r}_2)\rangle$, the result is identically zero unless the following three conditions are simultaneously satisfied: $|\mathbf{r}_1-\mathbf{r}_2|<2r_c$, $|\mathbf{r}_1-\mathbf{r}_3|<2r_c$, and $|\mathbf{r}_2-\mathbf{r}_3|<2r_c$. A three-center molecular coordinate system is shown in Fig. 4. The $\hat{\sigma}$ ($\hat{\mathbf{z}}$) axis is along the axis of the bond charge,

$$\phi_\mu^{\mathrm{PAO}}(\mathbf{r}+\tfrac{1}{2}d_{\mathrm{BC}}\hat{\sigma})\phi_\nu^{\mathrm{PAO}}(\mathbf{r}-\tfrac{1}{2}d_{\mathrm{BC}}\hat{\sigma}) ,$$

and the $\hat{\pi}$ ($\hat{\mathbf{x}}$) axis is in the plane of the three centers. The origin lies at the bond-charge center, equidistant from the two atoms forming the bond charge. The bond charge is nonzero only in the region of intersection of the two spheres of radius r_c. The nonzero three-center integrals are written in the following form:

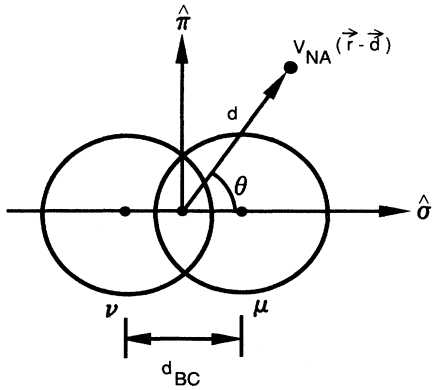

FIG. 4. The three-center molecular coordinate system used for the neutral-atom matrix elements. The three centers define the π-σ plane. The σ axis is the axis connecting the two orbitals μ and ν forming the bond charge, and the origin is midway between the two orbitals.

$$V_{\mu\nu}^{\mathrm{NA}}(d,d_{\mathrm{BC}},\theta)\equiv\langle\phi_{\mu}^{\mathrm{PAO}}(\mathbf{r}+\tfrac{1}{2}d_{\mathrm{BC}}\hat{\boldsymbol{\sigma}})|V_{\mathrm{NA}}(\mathbf{r}-\mathbf{d})|\phi_{\nu}^{\mathrm{PAO}}(\mathbf{r}-\tfrac{1}{2}d_{\mathrm{BC}}\hat{\boldsymbol{\sigma}})\rangle\ . \tag{24}$$

The problem is now one of classical electrostatics. The matrix element is the electrostatic interaction of a bond charge with the spherically symmetric potential from the atomic valence electron and pseudonuclear charges. The bond charge is neither spherically symmetric nor charge neutral. We therefore turn the problem around and view the matrix elment as that of the interaction of the pseudonuclear and spherically symmetric atomic valence charges with the electrostatic potential of the bond charge. The electrostatic potential $U_{\mu\nu}$ of the bond charge $\phi_{\mu}\phi_{\nu}$ is

$$U_{\mu\nu}(\mathbf{r})=\int\frac{\phi_{\mu}^{\mathrm{PAO}}(\mathbf{r}+\frac{1}{2}d_{\mathrm{BC}}\hat{\boldsymbol{\sigma}})\phi_{\nu}^{\mathrm{PAO}}(\mathbf{r}'-\frac{1}{2}d_{\mathrm{BC}}\hat{\boldsymbol{\sigma}})}{|\mathbf{r}-\mathbf{r}'|}d^{3}r'\ . \tag{25}$$

The kernel $1/|\mathbf{r}-\mathbf{r}'|$ is then expanded in associated Legendre polynomials $P_n^m(\cos\theta)$ in the standard way.[39] Only one value of m survives for a given type of matrix element. The potential can be written in the form

$$U_{\mu\nu}=\begin{array}{c} \\ s \\ \pi \\ \pi' \\ \sigma \end{array}\begin{array}{c} \begin{array}{cccc} s & \pi & \pi' & \sigma \end{array} \\ \begin{pmatrix} u_{ss} & \cos\phi\,u_{s\pi} & \sin\phi\,u_{s\pi} & u_{s\sigma} \\ \cos\phi\,u_{\pi s} & [u_{\pi\pi}+\cos(2\phi)u_{\pi\pi'}]/2 & \sin\phi\cos\phi u_{\pi\pi'} & \cos\phi\,u_{\pi\sigma} \\ \sin\phi\,u_{\pi s} & \sin\phi\cos\phi\,u_{\pi\pi'} & [u_{\pi\pi}-\cos(2\phi)\,u_{\pi\pi'}]/2 & \sin\phi\,u_{\pi\sigma} \\ u_{\sigma s} & \cos\phi\,u_{\sigma\pi} & \sin\phi\,u_{\sigma\pi} & u_{\sigma\sigma} \end{pmatrix} \end{array}, \tag{26a}$$

where the functions u are functions of r, and ϕ and θ' are the angles in spherical coordinates as defined by the molecular coordinate system of Fig. 4, where π and σ play the role of x and z coordinates, respectively. The functions $u_{\mu\nu}$ have the form

$$u_{\mu\nu}=\sum_{n=0}^{\infty}P_n^0(\cos\theta')\left[\frac{Q_{n0}^{\mu\nu}(r)}{r^{n+1}}+r^nB_{n0}^{\mu\nu}(r)\right] \tag{26b}$$

for (μ,ν) being (s,s), (σ,σ), or (π,π),

$$u_{\mu\nu}=\sum_{n=1}^{\infty}\frac{P_n^1(\cos\theta')}{n(n+1)}\left[\frac{Q_{n1}^{\mu\nu}(r)}{r^{n+1}}+r^nB_{n1}^{\mu\nu}(r)\right] \tag{26c}$$

for (μ,ν) being (s,π), or (σ,π), and

$$u_{\mu\nu}=\sum_{n=2}^{\infty}\frac{P_n^2(\cos\theta')}{(n+2)(n+1)n(n-1)}\left[\frac{Q_{n2}^{\mu\nu}(r)}{r^{n+1}}+r^nB_{n2}^{\mu\nu}(r)\right] \tag{26d}$$

for (μ,ν) equal to (π,π'). The matrix elements for (μ,ν) being (σ,s), (π,s), and (π,σ) have the same form as those for (s,σ), (s,π), and (σ,π), except that the former have an extra factor of $(-1)^{n+1}$, $(-1)^{n+1}$, and $(-1)^n$, respectively.

The functions $Q_{nm}^{\mu\nu}(r)$ and $B_{nm}^{\mu\nu}(r)$ depend on the bond-charge type (μ,ν) and have an interpretation similar to r-dependent charges, dipoles, and the like. For the special case of identical atoms forming the bond charge (the case of elemental Si that we treat here), the odd-n moments $Q_{nm}^{\mu\nu}$ and $B_{nm}^{\mu\nu}$ vanish for $(\mu,\nu)=(s,s)$, (σ,σ), (π,π), and (π,π'). The exact functional form of Q and B is easily found; for our purposes we only need to know that they are functions of r, the magnitude of the distance from the bond-charge center. The interaction of the bond-charge electrostatic potential $U_{\mu\nu}$ with the neutral-atom valence and pseudonuclear charges gives the matrix element $V_{\mu\nu}^{\mathrm{NA}}(d,d_{\mathrm{BC}},\theta)$ of Eq. (24). Since the neutral-atom charge is spherically symmetric, the matrix element V has the same basic form as the bond-charge electrostatic potential U. An important difference is that θ' and ϕ are no loner integration variables, but are the angular coordinates of the neutral atom; hence ϕ is zero (see Fig. 4). The matrix elements have the form

$$V_{\mu\nu}^{\mathrm{NA}}(d,d_{\mathrm{BC}},\theta)=\begin{array}{c} \\ s \\ \pi \\ \pi' \\ \sigma \end{array}\begin{array}{c} \begin{array}{cccc} s & \pi & \pi' & \sigma \end{array} \\ \begin{pmatrix} v_{ss} & v_{s\pi} & 0 & v_{s\sigma} \\ v_{\pi_s} & (v_{\pi\pi}+v_{\pi\pi'})/2 & 0 & v_{\pi\sigma} \\ 0 & 0 & (v_{\pi\pi}-v_{\pi\pi'})/2 & 0 \\ v_{\sigma s} & v_{\sigma\pi} & 0 & v_{\sigma\sigma} \end{pmatrix} \end{array}, \tag{27a}$$

where the functions v are

$$v_{\mu\nu}=\sum_{n=0}^{\infty} P_n^0(\cos\theta)q_n^{\mu\nu}(d,d_{\rm BC}) \tag{27b}$$

for (μ,ν) being (s,s), (σ,σ), or (π,π),

$$v_{\mu\nu}=\sum_{n=1}^{\infty}\frac{P_n^1(\cos\theta)}{n(n+1)}q_n^{\mu\nu}(d,d_{\rm BC}) \tag{27c}$$

for (μ,ν) being (s,π) or (σ,π), and

$$v_{\mu\nu}=\sum_{n=2}^{\infty}\frac{P_n^2(\cos\theta)}{(n+2)(n+1)n(n-1)}q_n^{\mu\nu}(d,d_{\rm BC}) \tag{27d}$$

for (μ,ν) equal to (π,π'). Again, the matrix elements for (μ,ν) being (σ,s), (π,s), and (π,σ) have the same form as those for (s,σ), (s,π) and (σ,π), except that the former have an extra factor of $(-1)^{n+1}$, $(-1)^{n+1}$, and $(-1)^n$, respectively.

These results reflect electrostatic interactions of the bond-charge distribution, which has monopole, dipole, quadrupole, and higher moments, with the spherically symmetric distribution of the neutral atom. It must be understood that our expansions are not asymptotic expansions, but hold even for small distances. Rather, the expansions are angular-momentum expansions. Asymptotically (large d or $d_{\rm BC}$), they are particularly simple—all $q_n\to 0$ since either the moment of the bond-charge goes to zero (large $d_{\rm BC}$), or the bond charge interacts with a neutral-atom distribution that has all vanishing moments (large d).

The significance of Eqs. (27a)–(27d) is that the matrix elements depend on two distances, d and $d_{\rm BC}$, through the functions q_n, and the angular dependence is analytic. The dependence on $d_{\rm BC}$ is implicit in the functions Q and B of Eqs. (26b)–(26d). Analytic expressions involving integrals over the bond charges can be found, but we choose an easier scheme. We truncate the series after $n=4$, so for each relevant value of (μ,ν) we have at most five functions, q_0, q_1, q_2, q_3, and q_4. For fixed d and $d_{\rm BC}$, θ is varied over five angles and the electrostatic interaction is evaluated exactly by performing the three-dimensional integral in Eq. (24). This is done at the five angles given by $\cos\theta=0$, $1/\sqrt{3}$, $-1/\sqrt{3}$, $\sqrt{3/5}$, and $-\sqrt{3/5}$. The five functions q_n at the chosen value of d and $d_{\rm BC}$ are determined from five equations in five unknowns. The process is repeated over a grid of values of d and $d_{\rm BC}$ up to $2r_c$. Past $2r_c$, the matrix elements must identically be zero. In this way, the matrix elements $V_{\mu\nu}^{\rm NA}(d,d_{\rm BC},\theta)$ are determined for any geometry by interpolating on the two-dimensional grid for d and $d_{\rm BC}$, and analytically evaluating the angular dependence. Derivatives are also easily handled. The final transformation from molecular coordinates to the fixed "crystal" coordinate system is handled by a unitary transformation. Since they are three-center integrals, the simple Koster-Slater tables re not appropriate. The entire procedure has been found to be very fast in practice. The only time-consuming part is setting up the two-dimensional grid, which may involve $\sim 10k$ three-dimensional integrals. This, however, is a one-time cost.

There is a special case when the neutral atom resides on one of the atoms forming the bond charge. These matrix elements are large and are computed without approximation. Since they are two-center integrals, they are computed on a one-dimensional grid as described for the kinetic and overlap matrix elements. Another special case occurs when the two atoms forming the bond charge are the same ($d_{\rm BC}=0$). These two-center integrals are also calculated exactly on a one-dimensional grid in a similar manner.

C. Nonlocal pseudopotential matrix elements

In this subsection a description is given of the method used to determine the matrix elements of the nonlocal pseudopotential. Choosing the origin to lie at the origin of the pseudopotential, the matrix elements are

$$V_{\mu\nu}^{\rm NL}(\mathbf{r}_1,\mathbf{r}_2)=\langle\phi_\mu^{\rm PAO}(\mathbf{r}-\mathbf{r}_1)|V_{\rm NL}(r)|\phi_\nu^{\rm PAO}(\mathbf{r}-\mathbf{r}_2)\rangle\ . \tag{28}$$

The nonlocal pseudopotential has the form of Eq. (6),

$$V_{\rm NL}(r)=\sum_{l=0}^{2}V_l(r)\hat{P}_l\ .$$

Matrix elements of the nonlocal potential are generally a difficult part of pseudopotential calculations, and local pseudopotentials have been substituted in the more difficult calculations to simplify them.[25,26] We present here an exact method for determining the matrix elements between localized orbitals which makes the evaluation of these matrix elements one of the simpler steps in the calculation. Our method does not depend on any particular form of the orbitals or of the form of the radial potentials V_l. It is convenient to work with angular-momentum states (instead of Cartesian states s,p_x,p_y,p_z) for the orbitals:

$$\phi_{lm}(\mathbf{r})=R_l(r)Y_{lm}(\Omega_r)\ . \tag{29}$$

The angular-momentum projection of the atomic orbitals is most easily carried out in momentum space

$$\hat{P}_L\phi_{lm}^{\rm PAO}(\mathbf{r}-\mathbf{r}_1)=\hat{P}_L\frac{1}{(2\pi)^2}\int\phi_{lm}^{\rm PAO}(\mathbf{q})e^{i\mathbf{q}\cdot(\mathbf{r}-\mathbf{r}_1)}d^3q$$

$$=\frac{1}{2\pi^2}\sum_{M=-L}^{L}i^L Y_{LM}(\Omega_r)\int\phi_{lm}^{\rm PAO}(\mathbf{q})j_L(qr)Y_{LM}(\Omega_q)e^{-i\mathbf{q}\cdot\mathbf{r}_1}d^3q\ . \tag{30}$$

The matrix element of the nonlocal potential becomes

$$V_{lm,l'm'}^{\rm NL}(\mathbf{r}_1,\mathbf{r}_2)=\frac{1}{4\pi^4}\sum_{L=0}^{2}\sum_{M=-L}^{L}\int_0^\infty r^2\,dr\,V_L(r)A_{LM}^{lm}(r,\mathbf{r}_1)A_{LM}^{l'm'}(r,\mathbf{r}_2)\ ,$$

with

$$A_{LM}^{lm}(r,\mathbf{r})=\int\phi_{lm}(\mathbf{q})e^{-i\mathbf{q}\cdot\mathbf{r}}j_L(qr)Y_{LM}(\Omega_q)d^3q\ .$$

The three-dimensional integrals in A are expanded as

$$A_{LM}^{lm}(r,\mathbf{r}')=16\pi^2(-1)^l(-i)^L\sum_{k=-l}^{l}(-1)^{(l-k)/2}C_{L+k}(l,m;L,M)Y_{L+k,M-m}(\Omega_{r'})D_l^{L,k}(r,r')\ .$$

where the D's are one-dimensional integrals,

$$D_l^{L,k}(r,r')=\int_0^\infty R_l(q)j_L(qr)j_{L+k}(qr')q^2\,dq\ , \tag{31}$$

and $R_l(q)$ is the Fourier transform of the radial part of the PAO's. The C factors arise from expressing the product of two spherical harmonics as a sum over spherical harmonics:

$$Y_{lm}^*(\Omega)Y_{l'm'}(\Omega)=\sum_{K=|l-l'|}^{l+l'}C_K(l,m;l',m')Y_{K,m'-m}(\Omega)\ .$$

These C factors are related to the Clebsch-Gordan coefficients and are given by the Gaunt formula[40]

$$C_K(l,m;l'm')=(-1)^m\left[\frac{(2l+1)(2l'+1)}{4\pi(2K+1)}\right]^{1/2}\langle l,l',-m,m'|l,l',K,m'-m\rangle\langle l,l',0,0|l,l',K,0\rangle\ . \tag{32}$$

The results are simplified by defining one-dimensional integrals J,

$$J_{ll'}^{Lkk'}(r_1,r_2)=\int_0^\infty dr\,r^2V_L(r)D_l^{L,k}(r,r_1)D_{l'}^{L,k'}(r,r_2)\ , \tag{33}$$

and by choosing a "molecular" coordinate system in which the $\hat{\sigma}$ axis is along $\mathbf{r}_1$ and the $\hat{\pi}'$ axis is perpendicular to the plane containing $\mathbf{r}_1$ and $\mathbf{r}_2$ as shown in Fig. 5. In this molecular coordinate system and using the definition of J, the matrix elements become

$$V_{lm,l'm'}^{\mathrm{NL}}(\mathbf{r}_1,\mathbf{r}_2)=64\sum_{L=0}^{2}\sum_{k=-l}^{l}\sum_{k'=-l'}^{l'}(-1)^\gamma C_{L+k}(l,m,L,0)C_{L+k'}(l',m';L,0)$$
$$\times Y_{L+k,-m}^*(\Omega_{r_1})Y_{L+k',-m'}^*(\Omega_{r_2})J_{ll'}^{Lkk'}(r_1,r_2)\ , \tag{34}$$

where $\gamma=(3l+3l'+2L-k-k')/2$. No approximations were made to obtain Eq. (34), and it is not dependent on the specific form used for the nonlocal pseudopotential and the wave functions. Although it appears formidable, Eq. (34) is actually quite simple since the Gaunt factors C, Eq. (32), are zero unless they satisfy the triangle condition.[41] The number of unique J integrals for Si is 15. These integrals are added with appropriate coefficients to give the complete 4×4 sp^3 matrix.[42] The average number of terms in Eq. (34) is seven, with a maximum of 12. Notice that the J integrals only depend on the two distances r_1 and r_2, and *not on their orientation.* All direction dependence is analytically contained in the spherical harmonics. In practice, values of r_1 and r_2 are chosen and the one-dimensional integral in Eq. (33) is computed. The integrand dies quickly since $V_L(r)$ is highly localized. The results are tabulated on a two-dimensional grid of r_1 and r_2 values, and an interpolation scheme is used during a molecular-dynamics simulation. The method is exact and can be used efficiently in a molecular-dynamics scheme.

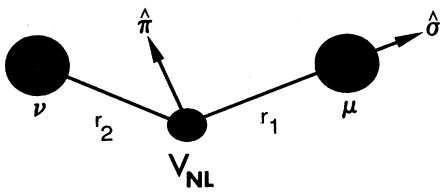

FIG. 5. The three-center coordinate system used for the nonlocal pseudopotential matrix elements. The three centers define the π-σ plane. The origin is taken to be the location of the nonlocal pseudopotential, and the σ axis is in the direction of $\mathbf{r}_1$.

D. Exchange-correlation matrix elements

Within the local-density approximation, the exchange and correlation (XC) energy, $\varepsilon_{\mathrm{XC}}(n)$, is a functional of the electron number density $n(\mathbf{r})$. The functional is nonlinear in n with the exchange part being

$$\varepsilon_X(n)=-\tfrac{3}{4}\frac{e^2}{\pi}(3\pi^2n)^{1/3}\ . \tag{35}$$

In principle, the matrix element of a function such as Eq. (35) can be obtained by evaluating the density at each $\mathbf{r}$ point and numerically computing the integral. However, this would be a very time-consuming step in a procedure such as a molecular-dynamics simulation. We therefore seek an approximation. In what follows, we illustrate by using the X/C energy, $\varepsilon_{\mathrm{XC}}(n)$. The procedure is identical for the XC potential, $\mu_{\mathrm{XC}}(n)$. Our approach is to determine an effective density $\bar{n}$ which changes in a linear way with the atoms nearby, and to use this density in a nonlinear way in the function $\varepsilon_{\mathrm{XC}}(\bar{n})$.

Let us consider a hopping matrix element where the orbitals are separated by a distance d. The results for the on-site matrix elements where d is zero will be given later. We search for the desired effective density $\bar{n}$ by expanding the functional about $\bar{n}$,

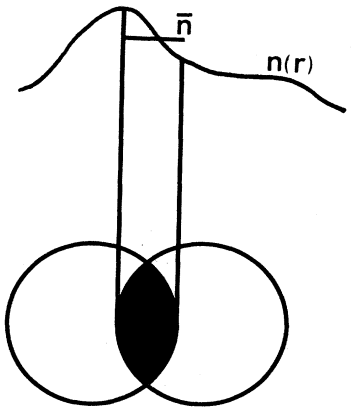

FIG. 6. Schematic diagram showing the determination of the effective density $\bar{n}$ from the bond charge at the density $n(\mathbf{r})$. The effective density $\bar{n}$ is the average of $n(\mathbf{r})$ weighted by the bond charge formed by the product of orbitals $\phi_\mu^{\mathrm{PAO}}\phi_\nu^{\mathrm{PAO}}$.

$$\varepsilon_{\mathrm{XC}}(n)=\varepsilon_{\mathrm{XC}}[\bar{n}+(n-\bar{n})]$$
$$=\varepsilon_{\mathrm{XC}}(\bar{n})+\varepsilon'_{\mathrm{XC}}(\bar{n})(n-\bar{n})+\varepsilon''_{\mathrm{XC}}(\bar{n})\frac{(n-\bar{n})^2}{2}+\cdots . \tag{36}$$

The matrix element of this functional is

$$\varepsilon_{\mu\nu}=\langle\phi_\mu^{\mathrm{PAO}}(\mathbf{r})|\varepsilon_{\mathrm{XC}}(n)|\phi_\nu^{\mathrm{PAO}}(\mathbf{r}-\mathbf{d})\rangle$$
$$\approx\varepsilon_{\mathrm{XC}}(\bar{n})S_{\mu\nu}+\varepsilon'_{\mathrm{XC}}(\bar{n})(n_{\mu\nu}-\bar{n}S_{\mu\nu})$$
$$+\tfrac{1}{2}\varepsilon''_{\mathrm{XC}}(\bar{n})[(n-\bar{n})^2]_{\mu\nu}+\cdots , \tag{37}$$

where $S_{\mu\nu}$ is the overlap and $n_{\mu\nu}$ is the matrix element of the density. Our choice of $\bar{n}$ is made by demanding that the series converge rapidly. We choose $\bar{n}$ so that the second term is identically zero, and the third term is minimized. These two conditions are met simultaneously by the choice

$$\bar{n}=n_{\mu\nu}/S_{\mu\nu} . \tag{38}$$

The effective density we choose is different for each matrix element. The result of Eq. (38) is that the effective density $\bar{n}$ is an average over the bond charge given by the product of orbitals $\phi_\mu^{\mathrm{PAO}}\phi_\nu^{\mathrm{PAO}}$. The effective density $\bar{n}$ is the local density weighted by the structure, special extent, and geometry of the bond charge. This is shown schematically in Fig. 6. This procedure has the feature of importance sampling, since the density is weighted more heavily when the bond charge is high. The denominator of Eq. (38) is simply a normalization factor for the weighting.

The above procedure is not defined if the overlap vanishes, such as, for instance, between an s and a p_π orbital. A matrix element of the XC energy between two such orbitals is not necessarily zero in low-symmetry situations due to three-center effects. In such cases, with the origin of coordinates at the center of the bond charge, n is replaced by

$$n(\mathbf{r})=\bar{n}+\mathbf{p}_\perp\cdot\mathbf{r}_\perp+\mathbf{r}_\perp\cdot\mathbf{Q}_\perp\cdot\mathbf{r}_\perp , \tag{39}$$

where $\mathbf{r}_\perp$ is the component of the position vector perpendicular (in the $\hat{\pi}$-$\hat{\pi}'$ plane) to the axis of the bond charge. The first term is an average monopolelike density, $\mathbf{p}_\perp$ allows for a dipole, and $\mathbf{Q}_\perp$ is a 2×2 symmetric, traceless, quadrupolelike tensor. We include only the first nonvanishing term, and determine $\mathbf{p}_\perp$ and $\mathbf{Q}_\perp$ by a similar criterion as that used for $\bar{n}$. The result is

$$\varepsilon_{\mu\nu}=\begin{array}{c} \\ s \\ \pi \\ \pi' \\ \sigma \end{array}\begin{array}{c} \begin{array}{cccc} s & \pi & \pi' & \sigma \end{array} \\ \begin{pmatrix} \varepsilon(\bar{n}_{ss})S_{ss} & 0 & 0 & \varepsilon(\bar{n}_{s\sigma})S_{s\sigma} \\ 0 & \varepsilon(\bar{n}_{\pi\pi})S_{\pi\pi} & 0 & 0 \\ 0 & 0 & \varepsilon(\bar{n}_{\pi\pi})S_{\pi\pi} & 0 \\ \varepsilon(\bar{n}_{\sigma s})S_{\sigma s} & 0 & 0 & \varepsilon(\bar{n}_{\sigma\sigma})S_{\sigma\sigma} \end{pmatrix} \end{array}$$

$$+\begin{array}{c} \\ s \\ \pi \\ \pi' \\ \sigma \end{array}\begin{array}{c} \begin{array}{cccc} s & \pi & \pi' & \sigma \end{array} \\ \begin{pmatrix} 0 & \varepsilon'(\bar{n}_{s\pi})n_{s\pi} & \varepsilon'(\bar{n}_{s\pi})n_{s\pi'} & 0 \\ \varepsilon'(\bar{n}_{\pi s}n_{\pi s} & \varepsilon'(\bar{n}_{\pi\pi})\dfrac{(n_{\pi\pi}-n_{\pi'\pi'})}{2} & \varepsilon'(\bar{n}_{\pi\pi})n_{\pi\pi'} & \varepsilon'(\bar{n}_{\pi\sigma})n_{\pi\sigma} \\ \varepsilon'(\bar{n}_{\pi s})n_{\pi s} & \varepsilon'(\bar{n}_{\pi\pi})n_{\pi\pi'} & \varepsilon'(\bar{n}_{\pi\pi})\dfrac{(n_{\pi'\pi'}-n_{\pi\pi})}{2} & \varepsilon'(\bar{n}_{\pi\sigma})n_{\pi'\sigma} \\ 0 & \varepsilon'(\bar{n}_{\sigma\pi})n_{\sigma\pi} & \varepsilon'(\bar{n}_{\sigma\pi})n_{\sigma\pi'} & 0 \end{pmatrix} \end{array} . \tag{40}$$

The first matrix is the monopole contribution given by the procedure described concerning Eqs. (37) and (38) and exists between orbitals with nonvanishing overlap. The second matrix is a correction which includes dipole and quadrupole

effects. It not only exists between orbitals that have vanishing overlap, but also corrects some with nonvanishing overlap. The second matrix is proportional to matrix elements of the density itself, giving the matrix $\varepsilon_{\mu\nu}$ the correct structure in low-symmetry situations. The matrix given by Eq. (40) transforms properly under a coordinate transformation.

The form of the result for terms involving ε' is unique, but the precise value of $\bar{n}$ is not. We have chosen values of $\bar{n}$ for these ε' terms which coincide with those of Eq. (38) as much as possible, and have taken on-site averages in other cases. Our results for $\bar{n}$ are

$$\bar{n}_{\mu\nu}= \begin{array}{c} \\ s \\ \pi \\ \pi' \\ \sigma \end{array} \begin{array}{c} \begin{array}{cccc} s & \pi & \pi' & \sigma \end{array} \\ \begin{pmatrix} n_{ss}/S_{ss} & \bar{n}_A & \bar{n}_A & n_{s\sigma}/S_{s\sigma} \\ \bar{n}_A & \dfrac{n_{\pi\pi}+n_{\pi'\pi'}}{2S_{\pi\pi}} & \dfrac{n_{\pi\pi}+n_{\pi'\pi'}}{2S_{\pi\pi}} & \bar{n}_A \\ \bar{n}_A & \dfrac{n_{\pi\pi}+n_{\pi'\pi'}}{2S_{\pi\pi}} & \dfrac{n_{\pi\pi}+n_{\pi'\pi'}}{2S_{\pi\pi}} & \bar{n}_A \\ n_{\sigma s}/S_{\sigma s} & \bar{n}_A & \bar{n}_A & n_{\sigma\sigma}/S_{\sigma\sigma} \end{pmatrix} \end{array} , \tag{41}$$

$\bar{n}_A$ being an on-site average over sp^3 orbitals and over the two atoms,

$$\bar{n}_A=\tfrac{1}{8}\sum_{\mu}[\langle\phi_\mu^{\mathrm{PAO}}(\mathbf{r})|n|\phi_\mu^{\mathrm{PAO}}(\mathbf{r})\rangle + \langle\phi_\mu^{\mathrm{PAO}}(\mathbf{r}-\mathbf{d})|n|\phi_\mu^{\mathrm{PAO}}(\mathbf{r}-\mathbf{d})\rangle] . \tag{42}$$

We find that the XC matrix elements for the condensed-matter phases of Si in diamond, simple-cubic (sc), fcc, bcc, and β-tin phases are accurately given by Eq. (40). Comparing with the exact matrix elements computed near the volumes of minimum energy for each of these phases, we find errors which are $\sim 2\%$. Although we do not generally anticipate a need to correct for these small errors, they can largely be corrected if necessary. The error comes predominantly from neglecting the third term of Eq. (37) involving $(n-\bar{n})^2$, which are fluctuations of the density about $\bar{n}$. This quantity is positive definite, so that the third term acts to oppose the first. This occurs because $\varepsilon_x''(\bar{n})$ has a sign opposite to $\varepsilon_x(\bar{n})$. The first term thus tends to overestimate the matrix element. A measure of the fluctuation of the density is the quantity R,

$$R=n_A/\bar{n} , \tag{43}$$

where n_A is the average density inside the atomic volume without the additional weighting of the bond charge,

$$n_A=\int_{\Omega_c} n(\mathbf{r})d^3r/\Omega_c ,$$

and $\Omega_c=\frac{4}{3}\pi r_c^3$ is the atomic volume. For a constant density, the fluctuations vanish and R is unity. The fluctuation correction to the XC matrix elements can be incorporated empirically as

$$\varepsilon_{\mu\nu}(\text{corrected})=[1-C_\infty(R_{\mu\nu})]\varepsilon_{\mu\nu}(\text{uncorrected}) , \tag{44}$$

where the uncorrected matrix elements are those defined by Eq. (40). The function $C_\infty(R)$ was determined empirically by comparing with exact matrix elements for five Si phases and is shown in Fig. 7. We show C_∞ at different volumes (and hence R values). The chosen volumes for each phase correspond to the volume that minimizes the energy per atom, and a volume about 5% above and below it. Although there is scatter, the general trend is that the correction is about 2.5% in the low-density diamond phase (large fluctuations), and goes toward zero in the higher-density phases as R approaches unity. The effect of this approximation on the energetics of these systems will be considered in Sec. V. We have found this correction to have only a minor effect and generally feel it unnecessary. In particular, C_∞ has been obtained empirically by performing an exact calculation, which may not always be possible.

The on-site matrix elements are obtained in a way similar to that of the hopping matrix elements, but with two important differences. The first difference is that a $\hat{\sigma}$ axis cannot uniquely be defined, and all three directions must be treated equally. The second difference is that the overlap matrix elements are either zero or one. With these two differences taken into account, the on-site matrix elements are

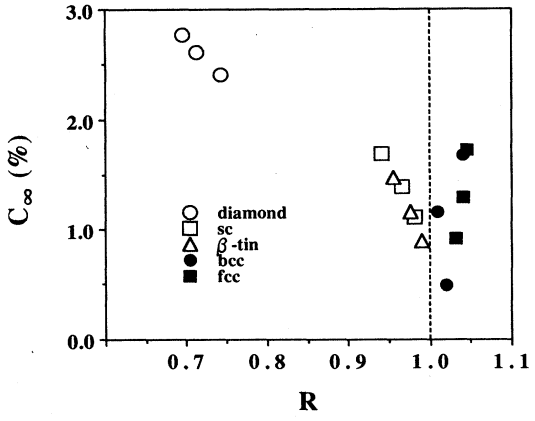

FIG. 7. The empirically determined exchange-correlation correction function C_∞ vs R for the largest hopping matrix element pp_σ in five condensed-matter phases of Si at different volumes. The quantity R is a dimensionless measure of density fluctuations and ideally C_∞ should approach zero as R approaches 1 from above or below. The three points for each crystal structure shows C_∞ at three different volumes. The vertical line is to highlight the expected symmetry about $R=1$.

$$
\varepsilon_{\mu\nu}=\begin{array}{c} \\ s \\ x \\ y \\ z \end{array}\begin{array}{c} \begin{array}{cccc} s & x & y & z \end{array} \\ \begin{pmatrix} \varepsilon(\bar{n}_s) & 0 & 0 & 0 \\ 0 & \varepsilon(\bar{n}_p) & 0 & 0 \\ 0 & 0 & \varepsilon(\bar{n}_p) & 0 \\ 0 & 0 & 0 & \varepsilon(\bar{n}_p) \end{pmatrix} \end{array}
$$

$$
+\begin{array}{c} \\ s \\ x \\ y \\ z \end{array}\begin{array}{c} \begin{array}{cccc} s & x & y & z \end{array} \\ \begin{pmatrix} 0 & \varepsilon'(\bar{n}_{sp})n_{sx} & \varepsilon'(\bar{n}_{sp})n_{sy} & \varepsilon'(\bar{n}_{sp})n_{sz} \\ \varepsilon'(\bar{n}_{sp})n_{sx} & \varepsilon'(\bar{n}_p)\left[\dfrac{2n_{xx}-n_{yy}-n_{zz}}{3}\right] & \varepsilon'(\bar{n}_p)n_{xy} & \varepsilon'(\bar{n}_p)n_{xz} \\ \varepsilon'(\bar{n}_{sp})n_{sy} & \varepsilon'(\bar{n}_p)n_{xy} & \varepsilon'(\bar{n}_p)\left[\dfrac{2n_{yy}-n_{zz}-n_{zz}}{3}\right] & \varepsilon'(\bar{n}_p)n_{yz} \\ \varepsilon'(\bar{n}_{sp})n_{sz} & \varepsilon'(\bar{n}_p)n_{xz} & \varepsilon'(\bar{n}_p)n_{yz} & \varepsilon'(\bar{n}_p)\left[\dfrac{2n_{zz}-n_{xx}-n_{yy}}{3}\right] \end{pmatrix} \end{array} , \tag{45}
$$

where $\bar{n}_s=n_{ss}$, $\bar{n}_p=(n_{xx}+n_{yy}+n_{zz})/3$, and $n_{sp}=(\bar{n}_s+\bar{n}_p)/2$. The quantities $n_{\mu\nu}$ are on-site matrix elements of the density,

$$n_{\mu\nu}=\langle \phi_\mu^{\mathrm{PAO}}(\mathbf{r})|n(\mathbf{r})|\phi_\nu^{\mathrm{PAO}}(\mathbf{r})\rangle \ .$$

Any coordinate system can be used to compute Eq. (45), as the result transforms properly under a unitary transformation. As for the hopping matrix elements, the 4×4 matrix of Eq. (45) can be constructed by adding in the contributions to $n_{\mu\nu}$ from different atoms in a *linear* way, and then using this linear result in the nonlinear functions ε and ε'. We have not attempted to add a C_∞ correction for the on-site matrix elements since they are more "atomiclike" and play a less important role in the bonding.

V. Hellmann-Feynman forces

The forces acting on an atom at position $\mathbf{R}_l$ are determined by taking the derivative of the total energy with respect to $\mathbf{R}_l$,

$$\mathbf{F}_l=-\frac{\partial E_{\mathrm{tot}}}{\partial \mathbf{R}_l}=-\left[\frac{\partial \varepsilon_{\mathrm{BS}}}{\partial \mathbf{R}_l}+\frac{\partial U_{\mathrm{SR}}}{\partial \mathbf{R}_l}+\frac{\partial \delta U_{\mathrm{XC}}}{\partial \mathbf{R}_l}\right] . \tag{46}$$

All of these derivatives can be taken easily in the current method, and the forces obtained are exact. This is to be contrasted with standard self-consistent calculations, which must be converged to a very high degree before the forces are truly correct, since the forces they are not determined by a variational principle. The short-ranged force gives a two-body central potential. The noncentral non-two-body forces are contained mainly in the band-structure force, although we show that the XC term also contains forces of this type.

The band-structure force is evaluated using a variation of the Hellmann-Feynman theorem,[43–45]

$$
\begin{aligned}
-\frac{\partial \varepsilon_{\mathrm{BS}}}{\partial \mathbf{R}_l}&=-2\sum_i \frac{\partial}{\partial \mathbf{R}_l}\langle \psi_i|h^0|\psi_i\rangle \\
&=-2\sum_{i,\mu,\nu,l_1,l_2} a_i^*(\mu,l_1)a_i(\nu,l_2) \\
&\qquad\times\left[\frac{\partial (h^0)_{\mu\nu}^{l_1l_2}}{\partial \mathbf{R}_l}-\varepsilon_i\frac{\partial S_{\mu\nu}^{l_1l_2}}{\partial \mathbf{R}_l}\right] \\
&=\sum_{\mu,\nu,l_1,l_2}\left[P_{\mu\nu}^{l_1l_2}\frac{\partial (h^0)_{\mu\nu}^{l_1l_2}}{\partial \mathbf{R}_l}-E_{\mu\nu}^{l_1l_2}\frac{\partial S_{\mu\nu}^{l_1l_2}}{\partial \mathbf{R}_l}\right] .
\end{aligned} \tag{47}
$$

where a_i are the linear combination of atomic orbitals (LCAO) coefficients of Eq. (1). In the last form we used a density matrix and an energy density matrix defined as

$$\rho_{\mu\nu}^{l_1l_2}=2\sum_{i\ \mathrm{occ}} a_i^*(\mu,l_1)a_i(\nu,l_2)$$

and

$$E_{\mu\nu}^{l_1l_2}=2\sum_{i\ \mathrm{occ}} \varepsilon_i a_i^*(\mu,l_1)a_i(\nu,l_2) \ . \tag{48}$$

With the exception of the XC potential, the Hamiltonian h^0 is a sum of contributions from isolated atoms, so that the derivative of h^0 is a sum of derivatives coming from one-, two-, and three-center terms. These derivatives, as well as the overlap derivatives, are easily evaluated using the grids described in Sec. IV. It should be noted that the derivatives we take are of the matrix elements themselves; we do not take matrix elements of derivatives as is done in the conventional Hellmann-Feynman theorem. Thus the Pulay[46] corrections are included exactly without additional effort. The size of the density matrices which are needed to compute the forces is determined by the orbital cutoff r_c. The density matrices can be evaluated by k-space techniques in periodic

systems, by direct summation of the eigenvalues and eigenvectors in finite systems such as molecules or clusters, or by Green's-function techniques for the defect subspace[47] or other hybrid technique. The derivatives of the XC matrix elements are not simply a sum of contributions from individual atoms. This causes no serious complication as we show for the XC correction $\delta U_{\rm XC}$.

The force from the short-range term $U_{\rm SR}$ gives a sum of two-body central potentials. The short-ranged potential can be written as a self-term and a two-body term,

$$U_{\rm SR}=-\sum_l U^0_{ee}(\mathbf{R}_l)+\tfrac{1}{2}\sum_{l,l'}{}' V_{\rm SR}(|\mathbf{R}_l-\mathbf{R}_{l'}|)\ , \tag{49}$$

where

$$U^0_{ee}(\mathbf{R}_l)=\frac{e^2}{2}\int\int\frac{n_{\rm atom}(\mathbf{r}-\mathbf{R}_l)n_{\rm atom}(\mathbf{r}-\mathbf{R}_l)}{|\mathbf{r}-\mathbf{r}'|}d^3r\,d^3r' \tag{50}$$

is the one-body, neutral-atom, Hartree self-energy of the charge density of the atom at $\mathbf{R}_l$, and

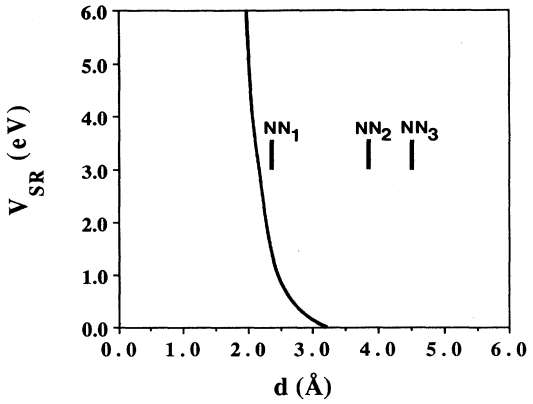

FIG. 8. The central two-body short-ranged repulsive potential $V_{\rm SR}$ vs separation between two Si atoms. Notice the strong potential at short distances (ultimately $1/r$), and the very fast decay. The first-, second-, and third-neighbor distances in crystalline Si are shown.

$$V_{\rm SR}(|\mathbf{R}_l-\mathbf{R}_{l'}|)=e^2\left[\frac{Z_lZ_{l'}}{|\mathbf{R}_l-\mathbf{R}_{l'}|}-\int\int\frac{n_{\rm atom}(\mathbf{r}-\mathbf{R}_l)n_{\rm atom}(\mathbf{r}-\mathbf{R}_l)}{|\mathbf{r}-\mathbf{r}'|}d^3r\,d^3r'\right] \tag{51}$$

is a repulsive potential that is the difference between the nuclear and electron Coulomb repulsions between the two neutral atoms at $\mathbf{R}_l$ and $\mathbf{R}_{l'}$. $V_{\rm SR}$ is short ranged, vanishing identically for $|\mathbf{R}_l-\mathbf{R}_{l'}|\geq 2r_c$. The short-ranged potential $V_{\rm SR}(|\mathbf{R}|)$ between two Si atoms is shown in Fig. 8. At small distances, the potential is singular. Notice that the potential only has a range of about 3.5 Å. This justifies the use of a first-neighbor model for the repulsive potential in calculations of others. The derivative of the one-body term vanishes, so that the short-ranged force becomes

$$-\frac{\partial U_{\rm SR}}{\partial\mathbf{R}_l}=-\sum_{l'}{}'\frac{\partial V_{\rm SR}(|\mathbf{R}_l-\mathbf{R}_{l'}|)}{\partial\mathbf{R}_l}\ ,$$

which is a simple sum of two-body central potentials.

The final force term is from the XC correction $\delta U_{\rm XC}$. This force is nearly a two-body force, but we show that the strength of the two-body force depends on the local environment. The XC energy from Eq. (14d) can be written in terms of on-site matrix elements,

$$\delta U_{\rm XC}=\sum_l\left[n_s(l)(\varepsilon_{\rm XC}-\mu_{\rm XC})_{ss}+\frac{n_p(l)}{3}[(\varepsilon_{\rm XC}-\mu_{\rm XC})_{xx}+(\varepsilon_{\rm XC}-\mu_{\rm XC})_{yy}+(\varepsilon_{\rm XC}-\mu_{\rm XC})_{zz}]\right]\ ,$$

where $n_s(l)$ $[n_p(l)]$ are the number of electrons in the s (p) states of the neutral atom, e.g., $n_s=2$ and $n_p=2$ for Si, and

$$(\varepsilon_{\rm XC}-\mu_{\rm XC})_{\mu\mu}=\langle\phi^{\rm PAO}_\mu(\mathbf{r}-\mathbf{R}_l)|[\varepsilon_{\rm XC}(n_0)-\mu_{\rm XC}(n_0)]|\phi^{\rm PAO}_\mu(\mathbf{r}-\mathbf{R}_l)\rangle\ . \tag{52b}$$

To differentiate Eq. (52a) involves differentiating Eq. (45). We will illustrate the result by considering the first term of Eq. (45) for ε_{ss}, the (s,s) matrix element of $\varepsilon_{\rm XC}$,

$$-\frac{\partial\varepsilon_{ss}}{\partial\mathbf{R}_l}=-\varepsilon'_{\rm XC}(n_{ss})\frac{\partial n_{ss}}{\partial_{\mathbf{R}_l}}\ , \tag{53}$$

where n_{ss} is the matrix element of the density. The density is a sum of densities on nearby atoms, so

$$-\frac{\partial\varepsilon_{ss}}{\partial\mathbf{R}_l}=\varepsilon'_{\rm XC}(n_{ss})\sum_{\mathbf{R}_{l'}}{}'-\frac{\partial}{\partial\mathbf{R}_l}\langle\phi^{\rm poa}_s(\mathbf{r}-\mathbf{R}_l)|n_{\rm atom}(\mathbf{r}-\mathbf{R}_{l'})|\phi^{\rm PAO}_s(\mathbf{r}-\mathbf{R}_l)\rangle\ . \tag{54}$$

This is a sum of two-body-like terms, but the coefficient, $\varepsilon'_{\rm XC}(n_{ss})$, depends on all the atoms in the vicinity since n_{ss} does. In any case, derivatives of terms such as those in Eq. (54) offer no particular difficulty as they are simple two-center integrals and are handled like the kinetic and overlap elements of Sec. IV A. Newton's third law is automatically satisfied for these matrix elements since

$$\left[\frac{\partial}{\partial\mathbf{R}_l}+\frac{\partial}{\partial\mathbf{R}_{l'}}\right]\langle\phi^{\rm PAO}_s(\mathbf{r}-\mathbf{R}_l)|n_{\rm atom}(\mathbf{r}-\mathbf{R}_{l'})|\phi^{\rm PAO}_s(\mathbf{r}-\mathbf{R}_l)\rangle=0\ .$$

TABLE I. Bulk properties of Si computed with PAO's of radius $r_c = 5a_B$ and without the C_∞ correction of the exchange-correlation energy (see text) compared with experiment. The cohesive energy was computed using the exact LDA energy of the atom ($r_c \to \infty$). For the cohesive energy only, we also give the result with the C_∞ correction (in parentheses).

	Theory	Experiment
Bulk modulus (GPa)	90.9	98.8
Optic-mode frequency (10^{14}/s)	0.98	0.99
Cubic lattice constant (Å)	5.50	5.43
Cohesive energy (eV)	5.03 (4.50)	4.63

VI. TESTS AND APPLICATION

A. Tests of the method

We have tested the method in bulk Si (diamond phase), on other phases of crystalline Si, and on small Si clusters. In the work reported here we use sp^3 pseudo-atomic-orbitals of radius $5a_B$ (a third-neighbor model for bulk Si), the Ceperley-Alder exchange-correlation functional,[15,16] and Hamann-Schlüter-Chiang (HSC) prescribed pseudopotentials.[17] The calculations are all spin unpolarized; the theory, however, is not limited to this, nor is it limited to only sp^3 orbitals. Unless otherwise stated, we do not include the C_∞ correction to the exchange-correlation matrix elements.

In Table I are shown the computed bulk properties of Si compared with experiment. We find good agreement with experiment for the bulk modulus, optic-mode frequency, and lattice constant. Also shown is the cohesive energy, which is the energy difference between the ground states of the solid and of the atom. Errors in the cohesive energy are usually attributed mainly to errors in the atomic energy and not the solid. This is especially true here since the energy of the free atom is raised considerably (~ 2.7 eV) by confining the electrons to a radius of $r_c = 5a_B$. This error is virtually nonexistent in the solid (~ 0.2 eV) since the kinetic energy of confinement is released by electron hopping. We show in Table I the cohesive energy calculated using the correct energy of the atom (computed exactly in the self-consistent LDA and pseudopotential approximations with $r_c \to \infty$). The solid, however, is computed using the techniques described in this work with $r_c = 5a_B$. The values in the table reflect a 0.07-eV (Ref. 48) correction from the zero-point motion of the solid, and a 0.65-eV (Ref. 48) correction of the atomic energy due to spin-polarization effects. The cohesive energy is shown with and without the C_∞ correction to the XC hopping matrix elements. The agreement with experiment is quite good, indicating that the ground-state energy of the solid is well described.

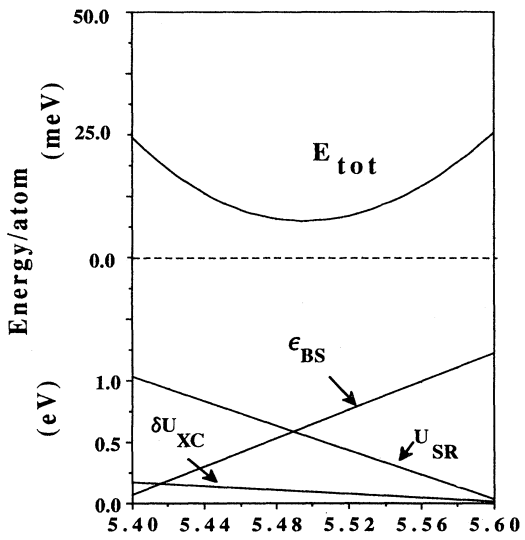

FIG. 9. The three separate components (ε_{BS}, δU_{XC}, and U_{SR}) to the total energy, and the total energy E_{tot} in Si vs cubic lattice constant a. A different constant was subtracted from each of the energies to get them on the same scale (see text). Notice the change in scale from the top and bottom parts of the figure.

In Fig. 9 we show a plot of the contributions to the total energy (band-structure energy, short-range energy, and exchange-correlation correction energy) versus cubic lattice constant a. Also included in this figure is the total energy for Si in the diamond structure. The energies on an absolute scale are obtained by adding -34.4, -84.8, 9.98, and -107.97 eV to ε_{BS}, U_{SR}, δU_{XC}, and E_{tot}, respectively. Note that no one contribution to the total energy dominates, and so all contributions must be determined accurately in order to get satisfactory results for the bulk modulus, equilibrium lattice constant, and so on.

The band structure of bulk Si is shown in Fig. 10. These bands are on an absolute energy scale. As in most tight-binding models, the valence bands are well described, but the conduction bands are not as accurately given. The conduction-band errors have little to do, however, with the energetics of the system. We find an indirect gap in the direction toward X, in agreement with experiment. However it is at $\sim 60\%$ of X instead of the experimental value of ~ 80–85%. The band gap we find is 1.74 eV compared with the experimental value of 1.17 eV. The LDA tends to underestimate the gap, but by us-

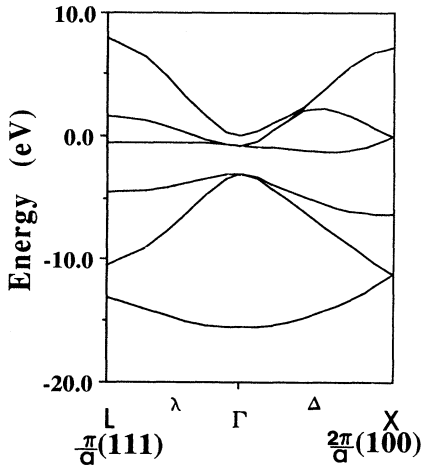

FIG. 10. The band structure of crystalline Si.

ing an sp^3 basis our method overestimates the gap.

A more stringent test of the theory is the phase diagram. We have investigated the total energy of the diamond, sc, β-tin, fcc, and bcc lattices as a function of volume. This range of phases gives both semiconductors and metals, and a variety of coordination numbers from 4 to 12. The axial ratio for β-tin was kept fixed at the experimental value.[49] We show the results in Fig. 11 as a function of reduced volume V/V_0, where V_0 is the experimental zero-pressure (diamond) volume. The density-dependent C_∞ correction factor in the XC (see Sec. IV D) for the hopping matrix elements has been included. For comparison, also shown in Fig. 11 are the theoretical results for the minimum-energy positions found by Yin and Cohen[50] rigidly shifted slightly vertically so that the minimum energies in the diamond phases agree. The Yin-Cohen calculations are self-consistent and were carried out using a rigorous expansion in a complete set (plane waves) of basis states. The agreement of our approximate method with the accurate calculations of Yin and Cohen is outstanding. All the major features are correct; the ordering is correct, the volumes of minimum energy are in good agreement, and the energy differences are in good agreement. This is particularly satisfying since the energy scale for these differences is ~ 0.01 Ry. These results contrast markedly with empirical tight-binding results, which give energy differences far too large, and completely unstable fcc and bcc lattices.[6]

In Fig. 12 we show the phase diagram for Si without the correction factor C_∞ used to produce Fig. 11. Note that all energies are lower in this figure because the XC energy has been slightly overestimated. The most significant feature is that the diamond structure is brought down the farthest since the overestimate is largest in this phase (see Fig. 7). Although the relative positions of the minimum energies have shifted slightly, the physics is still much the same. In particular, we find that the diamond structure is indeed the minimum-energy configuration and β-tin the next-lowest-energy, high-pressure phase.

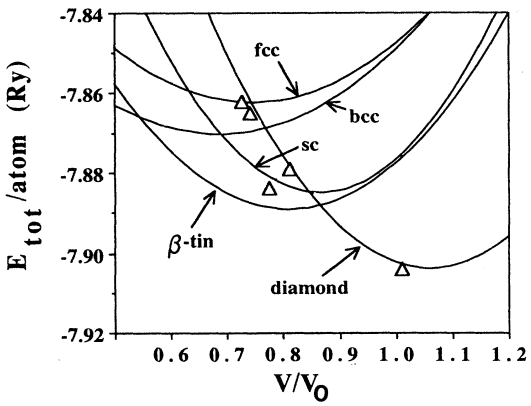

FIG. 11. Total energy of Si in diamond, β-tin, sc, bcc, and fcc crystalline phases as a function of reduced volume. The triangles indicate the minimum-energy configuration determined by Yin and Cohen. The triangles are not labeled, but have the same energy ordering as the minimum energy of each of our phases. The C_∞ correction has been added to the exchange correlation hopping matrix elements.

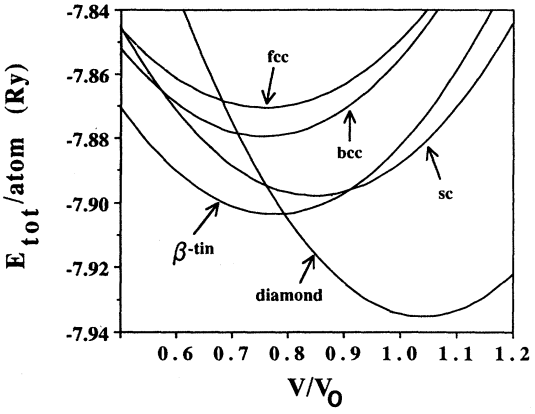

FIG. 12. Same as Fig. 11, but without the C_∞ correction.

The method has also been tested on a "low-density phase," the Si_2 molecule. Here the density variation is much greater than in the solid phases and is a more stringent test of our approximate form of the XC.

We have determined the total energy of the Si_2 molecule versus separation and obtain a minimum-energy configuration at $d=2.27$ Å and a vibrational mode at $\omega=531$ cm^{-1} using the uncorrected effective density for XC. These values compare well with experimental values of $d=2.24$ Å and $\omega=511$ cm^{-1}.[51] Correcting the XC energy by the density-dependent correction factor C_∞ results in a minimum-energy configuration at $d=2.29$ Å and a vibrational mode at $\omega=513$ cm^{-1}. The large reduction of distance between nearest neighbors, in going from bulk Si to the molecule is extremely well reproduced [0.11 Å experiment, 0.11 Å theory (uncorrected XC), and 11 Å theory (corrected XC)]. In Fig. 13 we show the eigenvalues of the one-electron Hamiltonian for Si_2 as a function of separation. In equilibrium (2.27 Å), the $1\pi_u$ level is four-fold degenerate (including spin) and contains two electrons. This figure is in excellent agreement with other calculations such as the spin-polarized results of Northrup *et al.*,[52] who find that the doubly degenerate

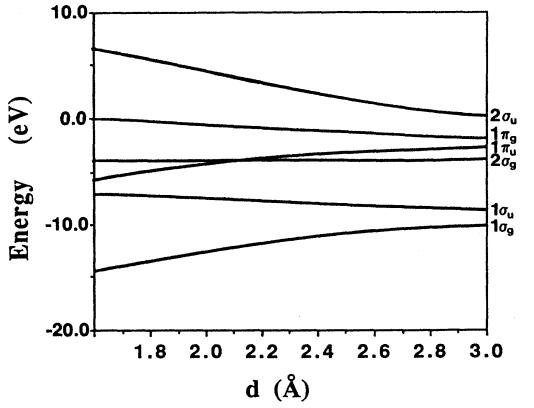

FIG. 13. One-electron eigenvalues for the Si_2 molecule as a function of intramolecular separation.

$1\pi_u$ level crosses the singly degenerate $2\sigma_g$ level at about $4.0a_B$ (2.12 Å), resulting in a new ground-state configuration at smaller separations. We find the $1\pi_u$ level crossing the $2\sigma_g$ level at $d=2.12$ Å.

B. Molecular-dynamics simulations

A simulated annealing study of the Si_3 molecule has been performed in order to determine the minimum-energy configuration. The simulated annealing was performed with 150 time steps of length 3.2 fs each. On each time step the Hellmann-Feynman forces on the atoms were calculated and the equations of motion,

$$\mathbf{F}_i = m_i \left[\frac{d^3\mathbf{r}_i}{dt^2} \right] \quad \{i=1,2,3\} ,$$

were solved to compute updated positions of the three atoms. To force the system to settle down to equilibrium, it was quenched by setting the velocities equal to zero on every other time step. The whole simulation takes a few CPU seconds on a convex C220.

The results of the calculation are shown in Fig. 14. We find Si_3 to form an isosceles triangle with the two equal sides of length 2.189 Å and an opening angle of 78.8°. Notice that it is quite far from the tetrahedral angle of bulk Si. These results are in very good agreement with much more rigorous calculations, such as those of Diercksen *et al.*,[53] who find $d=2.196$ Å and $\theta=80.6°$, or Grev *et al.*,[54] who find $d=2.160$ Å and $\theta=78.1°$.

A molecular-dynamics simulation of the simple vibrational spectrum of Si_2 at high and low "temperature" has also been performed. The motion of the atoms in the molecule was constrained so that the center of mass was stationary and the molecule had no angular momentum. The "temperature" is defined so that the thermal energy $\frac{1}{2}k_BT$ is the average kinetic energy of the relative coordinate. The Verlet[55,56] algorithm was used with a time step of 0.52 fs. The positions and velocities of the atoms were computed as a function of time from the quantum-mechanically derived forces, and the velocity autocorrelation function,

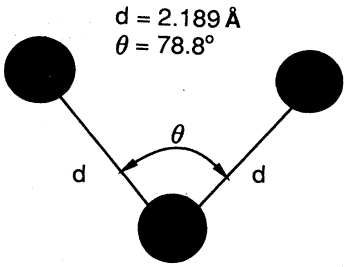

FIG. 14. The ground-state configuration found by simulated annealing of the Si_3 molecule.

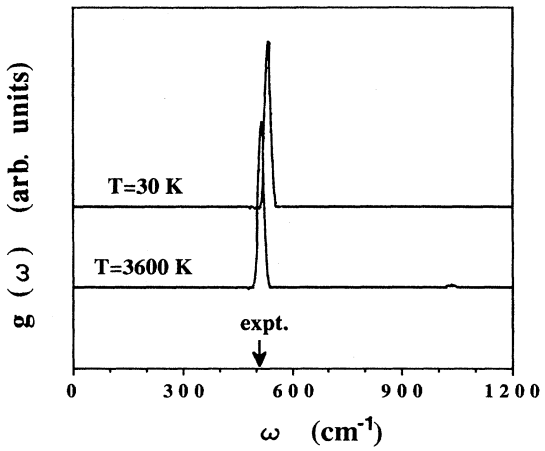

FIG. 15. Spectral density of Si_2 at low and high excitation levels. The frequency softens at high excitation and develops a small overtone feature. The experimental lowest-energy (quantized) excitation frequency is also shown for comparison.

$$g(t)=\sum_{n=1}^{2} \frac{\langle \mathbf{v}_n(t)\cdot\mathbf{v}_n(0)\rangle}{\langle \mathbf{v}_n(0)\cdot\mathbf{v}_n(0)\rangle} , \tag{55}$$

was determined. Here, n is the atom index and the $\langle\ \rangle$ indicate an ensemble average. The ensemble average is defined by

$$\langle f(t_i)f(0)\rangle \equiv \frac{1}{N-i+1}\sum_{m=0}^{N-i} f(t_{i+m})f(t_m) ,$$

where t_i is the time at step i $\{i=0,1,\ldots,N\}$.

The Fourier cosine transform of the autocorrelation function gives the spectral density $g(\omega)$,

$$g(\omega)=\Omega\frac{1}{2\pi}\int_0^T g(t)W(t)\cos(\omega t)dt , \tag{56}$$

where T is the total length of the simulation, $\Omega=2\pi/T$, and $W(t)$ is the Blackman window function[57] used to reduce finite-time sampling oscillations.

In Fig. 15 we present results for Si_2 for two temperatures, $T=30$ and 3600 K. We have used ~4000 times steps, so that the spectral density is broadened by a width of $\Omega\sim 20$ cm^{-1}. Figure 15 clearly shows the anharmonic effects of the mode softening at high excitation levels. Also note that a harmonic of the fundamental frequency begins to appear at high excitation levels. The intensity of the harmonics up to ninth (not shown) are comparable to those of the first harmonic. The frequency at the peak at low temperature from the molecular-dynamics simulation is the same as that obtained from the harmonic analysis of Sec. VI A. This simple simulation opens the door to straightforward first-principles simulations of the vibrational modes of more complex clusters and the in-

teraction and collision between clusters. This work is currently in progress and will be reported separately.

VII. CONCLUSIONS

The approximate electronic-structure method we have developed is physically motivated, fast and easy to use, and is entirely first principles. It requires no experimental input, and avoids complexities of more rigorous methods. It is executed in real space and requires no periodicity, and has been developed with applications to simulations, such as molecular dynamics, in mind. The method has been successfully tested on the physical properties of bulk material such as lattice constants, bulk moduli, optical-phonon frequencies, and phase stability, and on small Si clusters.

ACKNOWLEDGMENTS

We wish to thank the Office of Naval Research, U.S. Department of Defense, for their support under Contract No. ONR-N00014-85-K-0442. We wish to thank J. D. Dow, D. Drabold, and S. Klemm for their comments and suggestions. We also gratefully acknowledge the Notre Dame U.S. Defense Advanced Research Projects Agency–U.S. Office of Naval Research (DARPA/ONR) computer facility (N0530-0716-05 and N00014-89-J-1136).

[1]F. H. Stillinger and T. A. Weber, Phys. Rev. B **31**, 5262 (1985); M. I. Biswas and D. R. Hamann, Phys. Rev. Lett. **55**, 2001 (1985); J. Tersoff, *ibid.* **56**, 632 (1986); M. I. Baskes, *ibid.* **59**, 2666 (1987).

[2]W. Harrison, *Electronic Structure and the Properties of Solids* (Freeman, San Francisco, 1980).

[3]D. J. Chadi, Phys. Rev. B **29**, 785 (1984).

[4]P. Vogl, H. P. Hjalmarson, and J. D. Dow, J. Chem. Phys. Solids **44**, 365 (1983).

[5]V. Heine, in *Solid State Physics,* edited by H. Ehrenreich, F. Seitz, and D. Turnbull (Academic, New York, 1980), Vol. 35, p.1.

[6]A. T. Paxton, A. D. Sutton, and C. M. M. Nex, J. Phys. C **20**, L263 (1987).

[7]O. F. Sankey and R. E. Allen, Phys. Rev. B **33**, 7164 (1986).

[8]C. Z. Wang, C. T. Chan, and K. M. Ho (unpublished).

[9]D. A. Papaconstantopolous, *Handbook to the Bandstructure of Elemental Solids* (Plenum, New York, 1986).

[10]K. E. Newman and J. D. Dow, Phys. Rev. B **30**, 1929 (1984).

[11]W. C. Ford and C. W. Myles, Phys. Rev. B **38**, 1210 (1988).

[12]W. A. Harrison, Phys. Rev. B **27**, 3592 (1983).

[13]J. Robertson, Philos. Mag. **B47**, L33 (1983).

[14]P.-O. Löwdin, Adv. Quantum Chem. **5**, 185 (1970; J. Chem. Phys. **18**, 365 (1950).

[15]D. M. Ceperley and G. J. Alder, Phys. Rev. Lett. **45**, 566 (1980).

[16]J. Perdew and A. Zunger, Phys. Rev. B **23**, 5048 (1981).

[17]D. R. Hamann, M. Schlüter, and C. Chiang, Phys. Rev. Lett. **43**, 1494 (1979).

[18]G. B. Bachelet, D. R. Hamnn, and M. Schlüter, Phys. Rev. B **26**, 4199 (1982).

[19]R. W. Jansen and O. F. Sankey, Phys. Rev. B **36**, 6520 (1987).

[20]P. Hohenberg and W. Kohn, Phys. Rev. **136**, B864 (1964); W. Kohn and L. J. Sham, *ibid.* **140**, A1133 (1965).

[21]R. Car and M. Parrinello, Phys. Rev. Lett. **22**, 2471 (1985); Solid State Commun. **62**, 403 (1987).

[22]M. C. Payne, J. D. Joannopoulos, D. C. Allan, M. P. Teter, and D. H. Vanderbilt, Phys. Rev. Lett. **56**, 2656 (1986).

[23]R. Car and M. Parrinello, Phys. Rev. Lett. **60**, 204 (1988).

[24]P. Ballone, W. Andreoni, R. Car, and M. Perrinello, Phys. Rev. Lett. **60**, 271 (1988).

[25]M. C. Payne, P. D. Bristowe, and J. D. Joannopolous, Phys. Rev. Lett. **58**, 1348 (1987).

[26]M. Needels, M. C. Payne, and J. D. Joannopolous, Phys. Rev. Lett. **58**, 1765 (1987).

[27]M. C. Payne, M. Needels, and J. D. Joannopolous, Phys. Rev. B **37**, 8138 (1988).

[28]M. R. Pederson, B. M. Klein, and J. Q. Broughton, Phys. Rev. B **38**, 3825 (1988).

[29]J. Harris, Phys. Rev. B **31**, 1770 (1985).

[30]W. M. C. Foulkes, Ph.D. thesis, University of Cambridge, 1987, and unpublished.

[31]H. M. Polatoglou, and M. Methfessel, Phys. Rev. B **37**, 10403 (1988).

[32]F. Herman and S. Skillman, *Atomic Structure Calculations* (Prentice-Hall, Englewood Cliffs, NJ, 1963).

[33]R. W. Jansen and O. F. Sankey, Solid State Commun. **64**, 197 (1987); O. F. Sankey and R. W. Jansen, J. Vac. Sci. Technol. B **6**, 1240 (1988); R. W. Jansen, D. Wolde-Kidane, and O. F. Sankey, J. Appl. Phys. **64**, 2415 (1988).

[34]R. W. Jansen and O. F. Sankey, Phys. Rev. B **39**, 3192 (1989).

[35]R. W. Jansen, Ph.D. thesis, Arizona State University, 1987.

[36]A.-B. Chen and A. Sher, Phys. Rev. B **36**, 6603 (1982).

[37]E. P. Wigner and F. Seitz, Phys. Rev. **43**, 804 (1933); **46**, 509 (1934).

[38]J. C. Slater and G. F. Koster, Phys. Rev. **94**, 1498 (1954).

[39]J. D. Jackson, *Classical Electrodynamics* (Wiley, New York, 1962), p. 98.

[40]G. Baym, *Lectures on Quantum Mechanics* (Benjamin/Cummings, Menlo Park, CA, 1973), p. 365.

[41]M. Weissbluth, *Atoms and Molecules* (Academic, New York, 1978), p. 12.

[42]The technique works equally well for d^5 orbitals.

[43]H. Hellmann, *Einfuhrung in die Quantumchemie* (Franz Deutsche, Leipzig, 1937).

[44]R. P. Feynman, Phys. Rev. **56**, 340 (1939).

[45]B. M. Deb, Rev. Mod. Phys. **45**, 22 (1973).

[46]P. Pulay, Mol. Phys. **17**, 197 (1969); Theor. Chim. Acta **50**, 299 (1979).

[47]R. E. Allen and M. Menon, Phys. Rev. B **33**, 5611 (1986).

[48]W. R. L. Lambrecht and O. K. Andersen, Phys. Rev. B **34**, 2439 (1986).

[49]J. C. Jamieson, Science **139**, 762 (1963).

[50]M. T. Yin and M. L. Cohen, Phys. Rev. B **26**, 5668 (1982).

[51]D. E. Milligan and M. E. Jacox, J. Chem. Phys. **52**, 2594 (1970), and references therin.

[52]J. E. Northrup, M. T. Yin, and M. L. Cohen, Phys. Rev. A **28**, 1945 (1983).

[53]G. H. F. Diercksen, N. E. Gruner, J. Oddershele, and J. R. Sabin, Chem. Phys. Lett. **117**, 29 (1985).

[54]R. S. Grev, and H. F. S. Schaefer, Chem. Phys. Lett. **119**, 111 (1985).

[55]L. Verlet, Phys. Rev. **159**, 98 (1967).

[56]W. F. van Gunsteren, H. J. C. Berendsen, Mol. Phys. **34**, 1311 (1977).

[57]F. J. Harris, Proc. IEEE **66**, 51 (1978).